



HAL
open science

Controlled inline fluid separation based on smart process tomography sensors

Benjamin Sahovic, Hanane Atmani, Muhammad Awais A. Sattar, Matheus Martinez Garcia, Eckhart Schleicher, Dominique Legendre, Eric Climent, Rémi Zamansky, Annaïg Pedrono, Laurent Babout, et al.

► To cite this version:

Benjamin Sahovic, Hanane Atmani, Muhammad Awais A. Sattar, Matheus Martinez Garcia, Eckhart Schleicher, et al. Controlled inline fluid separation based on smart process tomography sensors. *Chemie Ingenieur Technik*, 2020, 92 (5), pp.554-563. 10.1002/cite.201900172 . hal-03181083

HAL Id: hal-03181083

<https://hal.science/hal-03181083v1>

Submitted on 25 Mar 2021

HAL is a multi-disciplinary open access archive for the deposit and dissemination of scientific research documents, whether they are published or not. The documents may come from teaching and research institutions in France or abroad, or from public or private research centers.

L'archive ouverte pluridisciplinaire **HAL**, est destinée au dépôt et à la diffusion de documents scientifiques de niveau recherche, publiés ou non, émanant des établissements d'enseignement et de recherche français ou étrangers, des laboratoires publics ou privés.



Open Archive Toulouse Archive Ouverte






OATAO is an open access repository that collects the work of Toulouse researchers and makes it freely available over the web where possible

This is a publisher's version published in: <https://oatao.univ-toulouse.fr/27536>

Official URL:

<https://doi.org/10.1002/cite.201900172>

To cite this version:


Sahovic, Benjamin and Atmani, Hanane  and Sattar, Muhammad Awais A. and Garcia, Matheus Martinez and Schleicher, Eckhart and Legendre, Dominique  and Climent, Éric  and Zamansky, Rémi  and Pedrono, Annaig  and Babout, Laurent and Banasia, Robert and Portela, Luis and Hampel, Uwe
Controlled inline fluid separation based on smart process tomography sensors.
(2020) *Chemie Ingenieur Technik*, 92 (5). 554-563. ISSN 0009-286X

Any correspondence concerning this service should be sent to the repository administrator: tech-oatao@listes-diff.inp-toulouse.fr

Controlled Inline Fluid Separation Based on Smart Process Tomography Sensors

Benjamin Sahovic^{1,*}, Hanane Atmani², Muhammad Awais A. Sattar³, Matheus Martinez Garcia⁴, Eckhart Schleicher¹, Dominique Legendre², Eric Climent², Remi Zamansky², Annaig Pedrono², Laurent Babout³, Robert Banasiak³, Luis M. Portela⁴, and Uwe Hampel^{1,5}

DOI: 10.1002/cite.201900172

 This is an open access article under the terms of the Creative Commons Attribution License, which permits use, distribution and reproduction in any medium, provided the original work is properly cited.

Today's mechanical fluid separators in industry are mostly operated without any control to maintain efficient separation for varying inlet conditions. Controlling inline fluid separators, on the other hand, is challenging since the process is very fast and measurements in the multiphase stream are difficult as conventional sensors typically fail here. With recent improvement of process tomography sensors and increased processing power of smart computers, such sensors can now be potentially used in inline fluid separation. Concepts for tomography controlled inline fluid separation were developed, comprising electrical tomography and wire mesh sensors, fast and massive data processing and appropriate process control strategy. Solutions and ideas presented in this paper base on process models derived from theoretical investigation, numerical simulations and analysis of experimental data.

Keywords: CFD simulation, Control systems, Electrical tomography, Inline fluid separation, Wire mesh sensor

Received: November 01, 2019; *revised:* February 21, 2020; *accepted:* March 11, 2020

1 Introduction

Separation processes are present in many industries. In particular, they are vital to the oil industry, e.g., in the petroleum exploration and refinement. In oil exploration, for instance, the separation of the crude oil from other components (water, gas and sand) in the flow coming from the well is achieved by exploiting the difference in the density of these elements. Density driven separation methods typically employ gravitational or centrifugal effects. Gravity tanks (such as settling tanks or three phase separators) are devices that rely on gravity to separate phases from a mixture, while cyclones take advantage of the centripetal force to achieve the separation. Fig. 1 shows simplified schematics of a gravitational separator (a) and a cyclone (b) on the example of oil water separation.

The vertical velocities of individual rising oil and settling water droplets inside a gravity tank are determined by the balance between the buoyancy, gravity and drag forces. Therefore, this balance determines the time scale of the separation process. Simultaneously, the flow continuously crossing the separator generates a horizontal motion of the particles, defining their residence time inside the device. A successful separation is achieved when the residence time is greater than the separation time. However, this leads to very large devices when small droplets need to be separated as their vertical velocities are low. In the petroleum industry, for instance, gravity separators may be up to 25 m in length and 3 m in diameter [1].

Cyclones are simple and robust alternatives to overcome the size problem of gravitational separators. These devices are designed to generate accelerations much higher than gravity (up to 100g) via a swirling of the mixture. The much higher driving force inside cyclones results in a tremendous decrease in the separation time, which allows a considerable reduction in the size of the equipment. The compactness of cyclones in relation to gravity tanks makes them especially attractive to offshore petroleum exploration, due to the

¹Benjamin Sahovic, Eckhart Schleicher, Prof. Dr. Ing. Uwe Hampel
b.sahovic@hzdr.de

Helmholtz Zentrum Dresden Rossendorf, Institute of Fluid Dynamics, Bautzner Landstraße 400, 01328 Dresden, Germany.

²Hanane Atmani, Dr. Dominique Legendre, Dr. Eric Climent, Dr. Remi Zamansky, Dr. Annaig Pedrono, Institut National Polytechnique de Toulouse, Institut de Mécanique des Fluides de Toulouse, Allée Emile Monso 6, 31029, Toulouse Cedex 4, France.

³Muhammad Awais A. Sattar, Dr. Laurent Babout, Dr. Robert Banasiak

Lodz University of Technology, Institute of Applied Computer Science, Stefanowskiego 18/22, 90 924 Łódź, Poland.

⁴Matheus Martinez Garcia, Dr. Luis M. Portela
Delft University of Technology, Department of Chemical Engineering, Van der Maasweg 9, 2629 HZ Delft, Netherlands.

⁵Prof. Dr. Ing. Uwe Hampel
Technische Universität Dresden, Chair of Imaging Techniques in Energy and Process Engineering, 01062 Dresden, Germany.

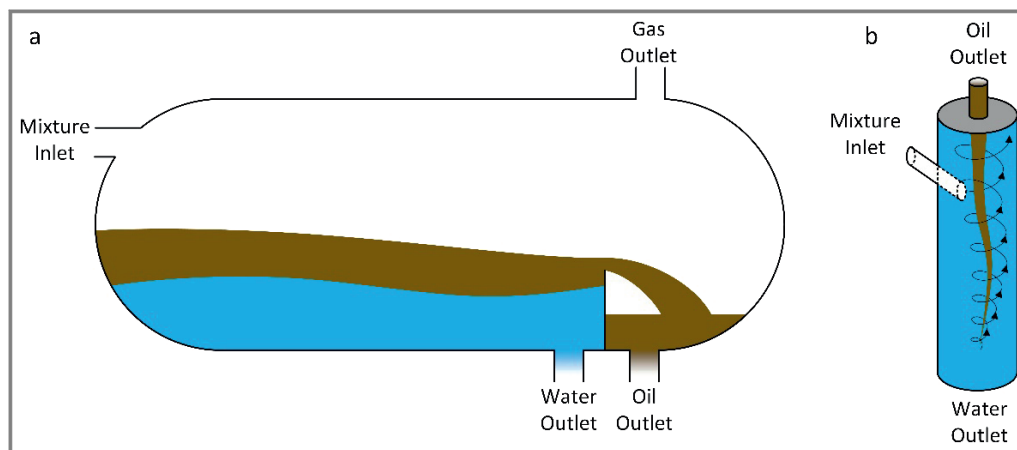


Figure 1. Common separator types used for oil water separation. a) Gravity tank, b) cyclone separator.

spatial limitation of the platforms [2, 3]. Moreover, cyclones are already being used in the petroleum industry, e.g., to remove oil from the water before discharging it into the ocean.

An inline fluid separator is a special type of cyclone separator. The difference is the flow direction of incoming fluids [5–7]. In the cyclonic separator (Fig. 1b), the multiphase flow is entering tangentially while in an inline fluid separator the fluid is entering axially (Fig. 2a). The inline fluid separator has a simpler design and its main parts are the pipe, a swirl element, a pickup tube and control valves.

However, some care must be taken when using cyclones and swirl separators. An oversized swirl motion shatters the oil droplets into smaller elements, which can lead to emulsions. The optimal operation points of swirl flow with respect to separation efficiency are strongly dependent on the individual flow rates (e.g., of oil and water) and on the size of the oil droplets at the inlet [4], which can vary in time. In addition, the swirl flow inside the swirl separator is intrinsically unsteady, leading to a time dependent and non optimal separation of the phases.

The unsteadiness of both the inlet flow conditions and the flow dynamics inside the swirl separator makes it desirable to have a real time control of the device. The complexity of the process and its short time constants are challenges to be overcome. In our concept, the control of the process will be achieved by using tomographic techniques that can provide rich real time information of the phase distribution upstream and downstream of the swirl element, and a simple reduced order model of the flow dynamics that can be used for real time computer control. To test this rather new approach we yet perform experimental designs and analysis on the example of air water separation, which is somewhat easier to do, but plan to extend the experimental part to oil water separation later on.

2 Concepts of a Controlled Inline Fluid Separator

Two potential concepts of a controlled inline fluid separator are illustrated in Fig. 2. These concepts are based partly on a fundamental design that was already developed in previous works of Slot [9], van Campen [4], Star [10] and Knöbel [11]. The core element of inline fluid separation is a swirl element inside a pipe that converts pressure into fluid angular momentum via its curved blades. The centrifugal effects, thus, push the heavier fluid towards the wall of the pipe, and the lighter fluid starts to accumulate around the pipe's center line. The lighter phase, which is gas here, is extracted either by a downstream pickup tube (design 1) or via a reverse flow through an extraction channel in the swirl element (design 2). The heavier phase (here water) leaves the separator straight ahead. Upstream and downstream of the swirl element there are tomographic sensors. In the experimental arrangement this will be wire mesh sensors upstream and an electrical resistance tomography (ERT) sensor downstream the swirl element.

The tomographic sensor upstream of the swirl element is actually a pair of wire mesh sensors, which allows measuring both gas fraction and gas velocity simultaneously. This provides the control system with information about the incoming flow. The ERT sensor monitors the gas vortex created by the swirl element. The choice of sensors is motivated by the following considerations. The wire mesh sensor is a very fast instrument with a typical image rate of 10 000 frames per second. It can obtain gas fraction distributions with high rate and accuracy. A further advantage is that it needs less data processing, as it requires, e.g., no image reconstruction. However, the sensor is intrusive and, hence, not suitable for the downstream gas core measurement, as it would create severe interaction with the gas core. There, the ERT sensor as a non intrusive instrument is much better suited. Moreover, ERT sensors can give some 3D information in principle. However, due to inherent relaxation time constants and image processing, the ERT sensor is somewhat

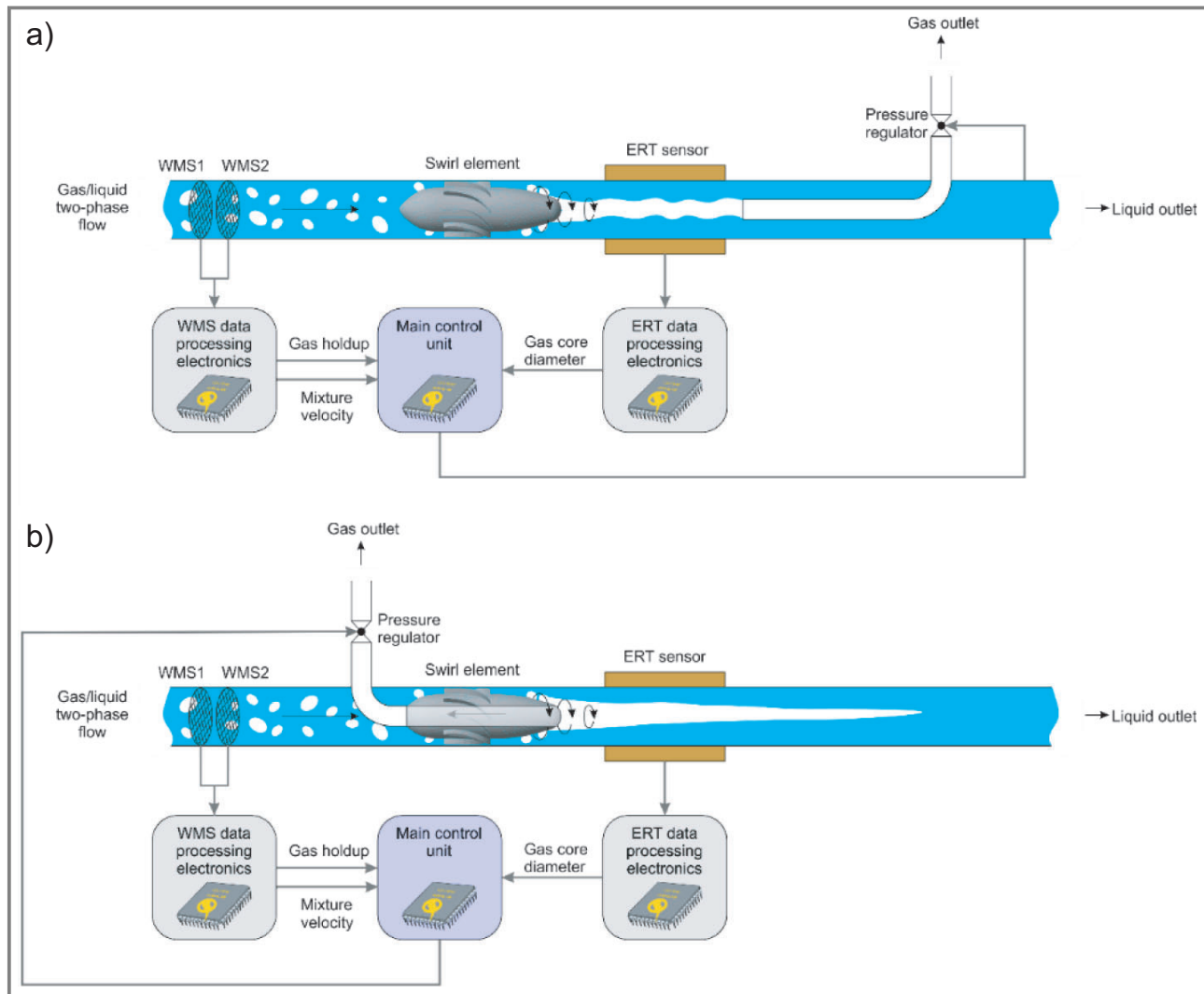


Figure 2. Two conceptual designs of a controlled inline fluid separator with tomographic imaging sensors and a controlled pressure regulator. a) Downstream gas extraction with a pickup tube; b) reverse gas extraction through the swirl element.

slower with a rate of about 10 frames per second. This has to be taken into account when designing the control part. More details of the tomographic imaging sensors are given below. The instrumental part is further complemented by pressure transducers upstream and downstream of the swirl element and at the outlets to yield additional dynamic pressure drop in formation for control. Furthermore, it is foreseen to capture the flow from the gas and liquid outlets and measure the gas carry under and the liquid carry over in each stream via scales. A CAD view of the test section is given in Fig. 3 for illustration.

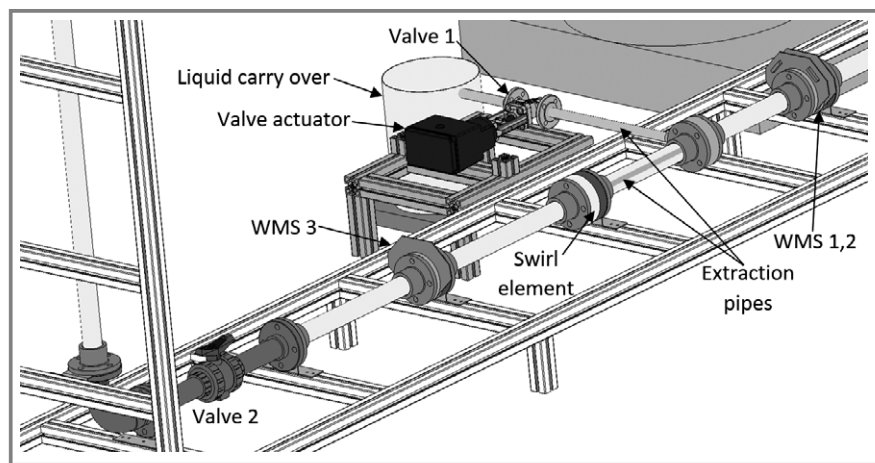


Figure 3. Experimental test section for the controlled inline fluid separator.

3 Control Strategy and System

Control of an inline fluid separator is a critical issue as the flow changes are fast and the imaging sensors produce some latency due to image processing and data reduction. Different strategies are being considered for the control step. As a classical controller a model predictive control concept is pursued (Fig. 4). It is based on a combined feedforward (predictive) action based on the wire mesh sensor signals and a feedback action basing on the ERT sensors operated at a lower frequency. Both the feedforward and the feedback part will be first implemented via black box transfer functions using sensitivity matrices obtained from experiments. A next step is to convert the black box into gray box models using the reduced order modeling described below. Later an extension to other controller types, such as controllers based on deep neural networks is envisaged.

4 Wire-Mesh Sensors

A wire mesh sensor consists of two planes of parallel wires placed in a pipe cross section [13]. They are separated by a short distance and arranged so that they form an angle of 90° to each other. The phase fraction (ratio of air to water) in the crossing points is obtained via electrical conductivity by successively applying voltages to wires of one plane and measuring electrical current flow to wires of the second plane. The image acquisition rate is 10 000 frames per second and the spatial resolution of the sensors is ~3 mm. Fig. 5 shows a photograph of the wire mesh sensors used in this study.

The fundamental parameter received from the wire mesh sensor is the local gas fraction ε in each wire crossing. From that, the total cross sectional gas fraction over time can be computed, which is

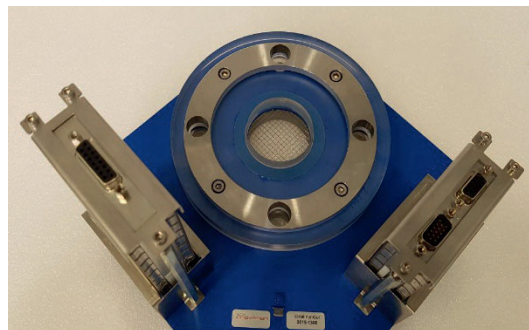


Figure 5. Wire mesh sensor.

$$\varepsilon(t_n) = \sum_i \sum_j a_{i,j} \varepsilon_{i,j}(t_n) \quad (1)$$

Here, $\varepsilon_{i,j}$ is the gas fraction in crossing point (i, j), $a_{i,j}$ are weights associated with the crossing points and t_n is the temporal sampling point. The $a_{i,j}$ mainly account for the round boundary of the wire grid.

Gas phase velocity can be obtained with a pair of two wire mesh sensors mounted adjacent to each other with a small axial displacement in the pipe (Fig. 6). To do this, the cross sectional averaged gas fraction readings from both sensors are cross correlated giving the cross correlation sequence

$$X(k) = \sum_n \varepsilon_1(t_n) \varepsilon_2(t_{n+k}) \quad (2)$$

Cross correlation is practically done via fast Fourier transformation (FFT). Its maximum value Δk gives the discrete temporal displacement for maximal similarity. Eventually, the average gas phase velocity \bar{u}_g is then computed as

$$\bar{u}_g = \frac{\Delta L}{\Delta k \Delta T} \quad (3)$$

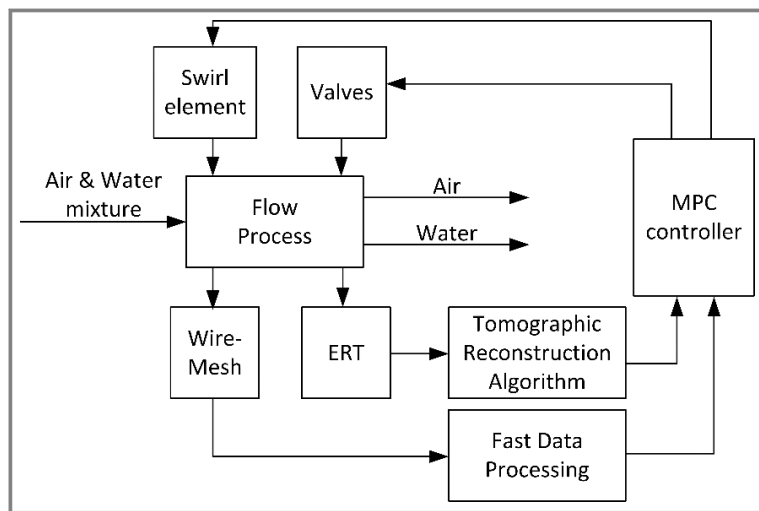


Figure 4. Generic control concept for the inline fluid separator.

with $\Delta T = 1/f_s$ being the sampling time step, f_s being the sampling frequency and ΔL being the axial distance between the two sensors. Both gas fraction and gas velocity calculation have been implemented into a fast FPGA hardware for online data processing to provide this information to the control system.

Experiments were performed at Helmholtz Zentrum Dresden Rossendorf to study the relationship between upstream and downstream behavior of the two phase flow in an inline fluid separator using wire mesh sensor upstream and a camera to observe the gas core downstream. In the investigations it was found that the gas core average diameter is correlated with inlet gas fraction within an uncertainty band of $\pm 15\%$ [14]. This proved that the wire mesh sensor can be used as a predictor for the forward control.

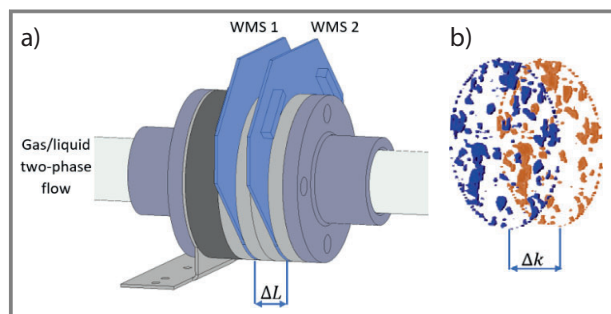


Figure 6. a) A pair of wire mesh sensors used for gas phase velocity measurement mounted with axial distance ΔL in the flow loop; b) cross sectional images of largest cross correlational similarity having a discrete temporal spacing Δk .

5 ERT Sensor

For tomographic imaging in the gas core region, electrical resistance tomography (ERT) is applied. This sensor technology was first introduced for medical applications in 1984 [16]. Recently, this tomography variant has been further developed for process imaging and monitoring [17, 18]. The two most common modalities are electrical capacitance tomography (ECT) and electrical resistance tomography (ERT). As we deal with a conducting liquid, ERT is used.

Here, the main focus is on the detection of the gas vortex and the measurement of its diameter. The tomography principle consists in retrieving cross sectional information of a media in a noninvasive way [15]. Being noninvasive in this region is very important as an intrusive sensor may disturb the flow and, hence, separation efficiency. A conventional ERT system is composed of three main parts: (i) sensor, (ii) data acquisition electronics and (iii) software for image reconstruction and visualization [19]. ERT sensors are used to obtain conductivity distribution of the flowing mixture and this is achieved by placing sensing electrodes at the periphery of the flow domain, while remaining in contact with the targeted medium [20]. The special excitation measurement scheme, used to obtain pairwise electrical impedances and image reconstruction, is based on a forward model of electrostatic field propagation. A commercialized measurement system Flow Watch together with WebRoc imaging software from Rocsole Ltd. is being used within the inline separation demonstrator. The Flow Watch system applies a voltage injection current measurement scheme such that one electrode is used as excitation electrode V_1 (source electrode) and the remaining electrodes (sink electrodes) are used for measurement as shown in Fig. 7 [21], while V_0 is ground voltage.

The physical sensor comprises 16 stainless steel electrodes of 12 mm head diameter and 5 mm thread size per electrode. They are placed equidistantly on the inner surface of the pipe. In order to avoid cross talk, the electrodes are well separated by about 5.7 mm. Electrodes were placed

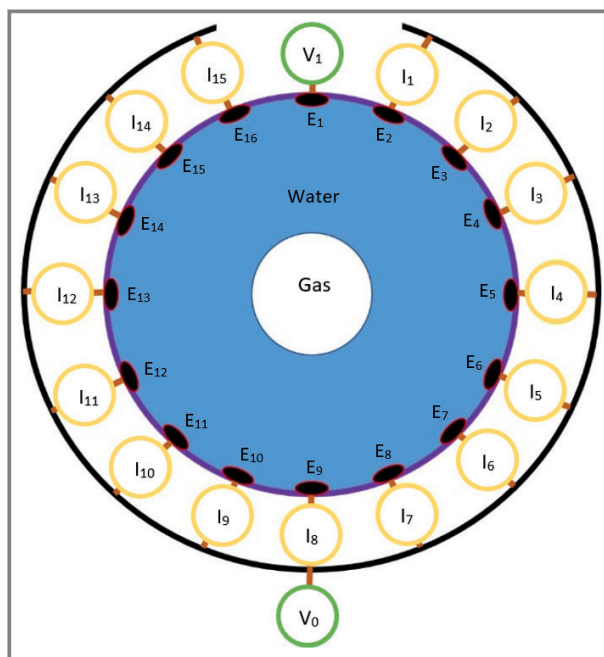


Figure 7. Schematics of an electrical resistance tomography front end with voltage injection current measurement protocol.

inside the pipe by drilling holes and are sealed using rubber sealing of 2 mm thickness. In order to match the impedance range of the signal with the target media the electrodes are connected to the electronics using a signal conditioning unit. This unit amplifies or damps the excitation voltage depending on the conductivity of the media under investigation. Coaxial RF connectors (MCX) were used for the connection between measurement electronics and the sensor. The Flow Watch system can be used for data acquisition and live image reconstruction. The data acquisition rate is 16 Hz and the image reconstruction rate is 4 Hz. For reconstruction, the dynamical Bayesian estimation method is employed. To observe the vortex, it is important to find an appropriate distance from the point of mixing to the point where stable vortex is formed. After some experimental analysis a distance of 500 mm downstream the tip of swirl element was found to be appropriate.

Preliminary experiments with tap water and air in a pipe of 90 mm diameter were conducted at the Liquid Gas Flow Research Facility of Tom Dyakowski Process Tomography Laboratory (Lodz University of Technology, Poland). The swirl element has been placed 1 m downstream the air and water injection point. Gas pressure and liquid flow rate were varied. Exemplary results for stable gas core are shown in Fig. 8 (pressure between 0.5 and 2.0 bar and liquid flow rates between $10 \text{ m}^3 \text{ h}^{-1}$ and $25 \text{ m}^3 \text{ h}^{-1}$). As image reconstruction is slow, current work aims at accelerating this by fast linear reconstruction schemes and applying a direct raw data analysis.

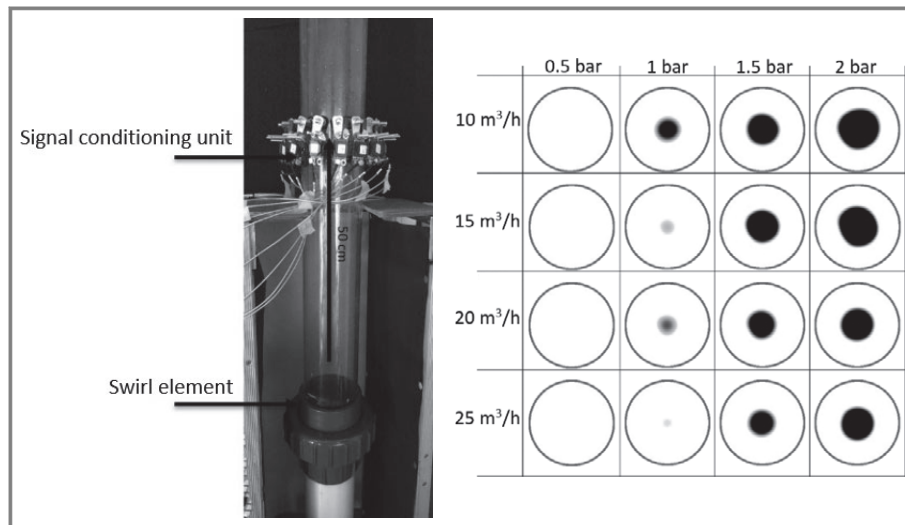


Figure 8. Left: single plane 16 electrodes ERT sensor placed above the swirl element for observing the gas vortex. Right: reconstructed images of the downstream gas core for different liquid flow rates and gas pressure. Light color corresponds to water and dark color to the gas core.

6 Fast Data and Image Processing Hardware

Recently, the increasing computational capabilities of computers to process massive data at high rate has made it possible to use tomographic sensors to quantify physical properties of a process in an industrial environment in real time. Tomographic sensors, like wire mesh sensors and ERT sensors, are generating large data sets. Two main parallel processing architectures are being used for concurrent computation. One of them is the field programmable logic array (FPGA) and the other is the graphic processing unit (GPU). Both differ in how an algorithm is being executed.

The parallel computing platform CUDA (computer unified device architecture) from Nvidia is used to prototype the algorithm for processing of tomographic sensor data. CUDA gives the ability to control a massively parallel processing environment and the algorithms have been tested on a Nvidia RTX 2070 mobile graphic card that has 2304 CUDA cores. Thus, the card can perform 2304 floating point operations in parallel per cycle.

An FPGA is a semiconductor device that can perform logical operations enabling the user to program its functions. The building block of an FPGA are wires, logic gates and registers. Modern FPGA, such as Arty 7 (Xilinx Inc.), have additional components, like memory blocks, transceivers, protocol controllers, clock generators and even a central processing unit (CPU), which greatly enhance data processing capability.

Eventually, the system will consist of a workstation combining GPU and FPGA capacity. The GPU will be a primary processing engine while the FPGA has a supporting role in the data acquisition. Thus, data from the wire mesh and tomography sensors will be acquired and processed in real time, so that information on flow properties can be pro-

vided in continuous time intervals for control. Therefore, the existing wire mesh sensor electronics is extended with an FPGA. A subsequent GPU is used to process the sensor data on a high level as well as compute and execute control actions. A similar concept exists for the ERT sensor and feedback control.

7 Process Modeling

7.1 Lumped-Parameter Reduced Order Modeling

Single phase bounded swirling flows have a case dependent axial velocity, a negligible radial velocity, and an azimuthal velocity that can be approximated to a solid

body rotation close to the center line and a decaying profile in the annular region [23, 24]. The axial, radial and azimuthal velocity profiles can be changed by controlling the flow at the two outlets and/or the geometry of the swirl element. These profiles are used in modeling to track the position of the particles along the flow by assuming a one way coupling between the phases [4, 25]. The small size of the particles allows the adoption of a tracing behavior (i.e., the velocity of the particle is assumed to be the fluid velocity) in the axial and tangential directions, while considering an additional slip velocity in the radial direction, caused by the centripetal acceleration. The procedure leads to the velocity of a single particle described by:

$$U_{p,r} = \left[\frac{4}{3} \left(1 - \frac{\rho_p}{\rho_l} \right) \frac{d_p}{r} \frac{1}{C_d} \right]^{\frac{1}{2}} U_\theta + U_r \quad (4)$$

$$U_{p,z} = U_z \quad (5)$$

$$U_{p,\theta} = U_\theta \quad (6)$$

Here, $U_{p,i}$ represents the components of the particle velocity, U_i represents the components of the fluid velocity, ρ_p and ρ_l are the densities of the particles and of the liquid phase, C_d is the drag coefficient and d_p is the dispersed phase diameter.

Fig. 9 illustrates a particle trajectory along the pipe for two different conditions. The top part shows a scenario where swirl motion is imposed on top of a uniform axial velocity, and no gravity effects are considered. There, the particle has a slip radial velocity in relation to the flow. This condition is modeled in Eq. (4) by the azimuthal velocity of the fluid, that induces a radial slip velocity of the particle.

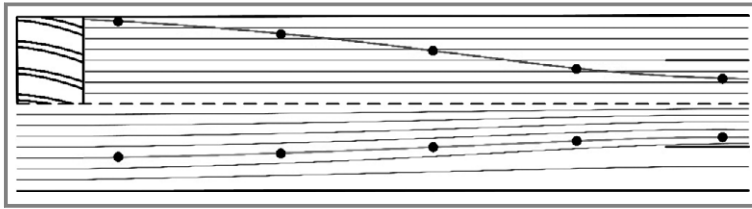


Figure 9. Particle trajectories inside the swirl tube. Top trajectory: swirl motion effects in the particle trajectory. Bottom trajectory: flow deviation effects in the particle trajectory.

The bottom part of Fig. 9 presents a condition where no azimuthal velocity is imposed and the particles follow the continuous phase streamlines, which are being deviated towards the pipe's center line. The total radial velocity of the particle in a contracting swirl is equal to the sum of individual responses of these effects, as evidenced in Eq. (4).

The motion of multiple particles is tracked along the pipe via a phase indicator function [26]. The expressions describing the dispersed phase motion are relatively simple, and the major challenge consists in obtaining reliable fluid velocity profiles as function of time and space.

The fluid dynamics of swirling flows is highly complex and unsteady, with, e.g., the precession of the vortex core and recirculation regions [27]. Moreover, the effect of the imposition of different flow splits on the dynamics of the flow is not known. The development of a simple reduced order model is fundamental for a successful real time process based control, and it is currently being explored.

7.2 Computational Fluid Dynamics

Most facilities or experimental rigs have limited range of operation in which they can perform desired experiments. Often, cost and time prevent excessive experimental studies. To support the modeling of the process on a very detailed fluid dynamics level, tools for computational fluid dynamics (CFD) are developed and applied.

In order to simulate the interaction between the two phase flow and the separator for the description of the gas core formation a hybrid Euler/Lagrange approach is developed. Considering that the scales are ranging from $O(1\text{ m})$, i.e., the length of the device, to $O(100\text{--}10\ \mu\text{m})$, i.e., the size of the smallest bubbles, the hybrid Euler/Lagrange method employs an immersed boundary method (IBM) to describe the geometry, a large eddy simulation (LES) for the turbulent flow, a Lagrangian tracking method for the bubble motion and a volume of fluid (VoF) method to describe the gas core region once bubble coalescence takes place after the swirl element. For the numerical simulations the IMFT in house CFD code JADIM [28] and its solvers for IBM, LES, Lagrangian, and VoF are used. For this study they need to be coupled. This is done via the mass and momentum conservation equations (Navier Stokes equations) in the following way:

$$\frac{\partial U_i}{\partial x_i} = 0 \quad (7)$$

$$\frac{\partial U_i}{\partial t} + \frac{\partial U_j U_i}{\partial x_j} = \frac{1}{\rho} \frac{\partial P}{\partial x_i} + \nu \frac{\partial^2 U_i}{\partial x_i \partial x_j} + g_i + F_i^{\text{IBM}} + F_i^{\text{VoF}} + F_i^{\text{LAG}} \quad (8)$$

Here ρ is the fluid density, U_i is the fluid velocity, P is the pressure, g_i is the gravity, ν is the kinematic viscosity and $F_i^{\text{IBM}}, F_i^{\text{VoF}}, F_i^{\text{LAG}}$ are the volumetric forcing coming from the IBM, VoF and Lagrangian methods, respectively. The Navier Stokes system of equations are discretized using a second order finite volume method. Time advancement is achieved through a third order Runge Kutta method for the advective and forcing terms and the Crank Nicolson method is used for the viscous stress. The incompressibility is satisfied at the end of each time step through a projection method.

In a first step the geometry is defined by using the immersed boundary method (IBM) to describe the separator and the pickup tube at the end of the pipe. The IBM, firstly introduced by Peskin [29], adds a volumetric force F^{IBM} , which is induced by the solid inside the calculation domain at the solid fluid interface level (Eq. (7)). The approach developed in JADIM is based on a solid volume fraction α^{IBM} equal to 1 in the solid and 0 outside. This method has been tested and used in JADIM for fixed and moving obstacles [30].

For turbulence modeling, the LES solver of JADIM [31] is chosen with a wall law to avoid the need of refined mesh next to the wall in order to limit the cost of the simulation. For that purpose, a specific treatment of the wall turbulent shear stress has been developed in connection with the IBM used for the solid description. The dynamic Smagorinsky model (DSM) considered here is the most adequate approach to simulate this kind of flow, allowing the calculation of a local Smagorinsky coefficient C_S used for the calculation of the eddy viscosity instead of fixing a constant. The filtered Navier Stokes equation then becomes:

$$\frac{\partial \bar{U}_i}{\partial t} + \frac{\partial \bar{U}_i \bar{U}_j}{\partial x_j} = \frac{1}{\rho} \frac{\partial \bar{P}}{\partial x_i} + \nu \frac{\partial^2 \bar{U}_i}{\partial x_j \partial x_j} - \frac{\partial \tau_{ij}^{\text{sgs}}}{\partial x_j} \quad (9)$$

where \bar{U}_i is the filtered velocity and τ^{sgs} is the subgrid scale stress tensor related to the Smagorinsky coefficient C_S through a subgrid eddy viscosity.

The dispersed flow is described using the Lagrangian tracking method [32] developed in JADIM. The bubbles are considered as spherical and their motion is described by solving their trajectory equation:

$$C_M \rho V_B \frac{dU_B}{dt} = \rho V_B g + F \quad (10)$$

where $C_M = 0.5$ is the added mass coefficient, V_B is the bubble volume and U_B their velocity. F is the force exerted by

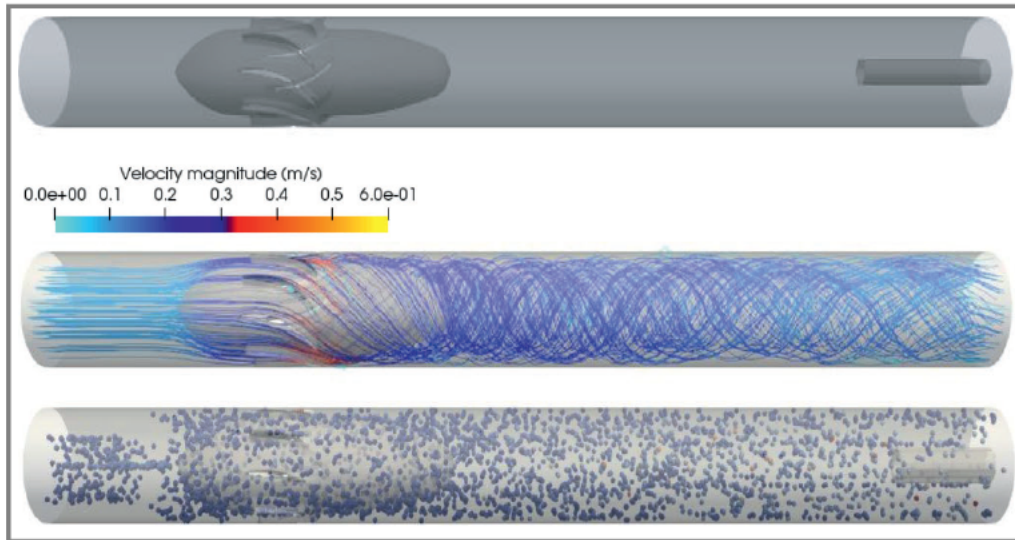


Figure 10. Top: geometry of the inline separator as used in the IBM simulation. Middle: streamlines of single phase flow for $Re = 4600$. Bottom: Two phase flow simulation using the coupling of immersed boundary method and Lagrangian tracking.

the fluid on the bubble and it contains the drag, lift, virtual mass and Tchen forces [32]. These forces are calculated using the fluid velocity interpolated at each bubble position. From F we deduce the resulting force F^{LAG} induced by the bubbles' motion inside the liquid. An elastic collision is introduced to describe the interaction between the bubbles and the IBM solid walls.

For simulating the gas core, a VoF method is chosen. It tracks the interface through the VoF function C , which stands for the volume fraction, i.e., $C = 1$ is pure gas phase and $C = 0$ is pure liquid phase. The motion of the gas liquid interface is then governed by the transport equation:

$$\frac{\partial C}{\partial t} + U_i \frac{\partial C}{\partial x_i} = 0 \quad (11)$$

The VoF [28] solver in JADIM does not need any interface reconstruction and is based on a flux corrected transport (FCT) solver. The capillarity contribution F' in Eq. (7) requires a specific treatment to avoid spurious current [28].

Let us consider a numerical domain of size $L_x \times L_y \times L_z$ on a Cartesian mesh made of $N_x \times N_y \times N_z$ nodes. The x direction corresponds to the axis of the pipe. The mesh is regular so that the grid size Δ is uniform along the three directions. The domain considered in the following examples is of size $L_x = 0.92$ m and $L_y = L_z = 0.1$ m. Fig. 10 displays the domain and a simulation result. The top figure shows the separator geometry as used with the IBM, the middle figure shows the streamlines of single phase flow for Reynolds number $Re = 4600$ and the bottom figure shows the bubbles tracked using the Lagrangian method and IBM.

8 Conclusion

In this paper, the novel idea of an inline fluid separator controlled with the help of a set of tomographic imaging sensors is introduced. For that, different basic designs are feasible and will be assessed and studied in the future. Many aspects have been considered in what would make the separator efficient including separator components, tomographic sensors, control system and data processing units. The control concept shall be based on a combined feedforward control with predictor using a wire mesh sensor and a feedback control using an ERT sensor. As inline fluid separation is a complex and fast process, it is difficult to build control algorithms on detailed physical modeling. Hence, a combination of process modeling using physical laws and black box models fitted by experimental data shall be applied.

This project has received funding from the European Union's Horizon 2020 Research and Innovation Program under the Marie Skłodowska Curie Grant Agreement No. 764902. We further acknowledge the active support of the TOMOCON Inline Fluid Separation Group by the following people: R. Belt (Total S.A.), J. Bos (Frames Group B.V.), P. Veenstra (Shell Global Solutions B.V.), R. Hoffmann (Linde AG), M. Trepte (Teletronic Rossendorf GmbH), A. Voutilainen (Rocsole Ltd.), R. Laborde (CERG Fluides S.A.S), M. J. Da Silva (Universidade Federal do Paraná Curitiba).

Symbols used

$a_{i,j}$	[]	weight coefficient of crossing points in a WMS
C_S	[]	local Smagorinsky coefficient
C_d	[]	drag coefficient
C_M	[]	mass coefficient
d_p	[mm]	dispersed phase diameter
f_s	[Hz]	sampling frequency
F_i^{IBM}	[N]	volumetric force from IBM method
F_i^{LAG}	[N]	volumetric force from Langragian method
F_i'	[N]	volumetric force from VoF method
g	[m s ⁻²]	earth's gravitational constant
k	[]	discrete temporal displacement
ΔL	[mm]	axial distance between sensors
P	[Pa]	pressure
Re	[]	Reynolds number
t_n	[]	temporal sampling point
ΔT	[s]	sampling time
$U_{p,i}$	[m s ⁻¹]	particle velocity
U_i	[m s ⁻¹]	fluid velocity
\bar{u}_g	[m s ⁻¹]	average gas phase velocity
V_1	[V]	voltage of source electrode
V_0	[V]	ground voltage

Greek letters

ε	[]	gas fraction
ρ	[kg m ⁻³]	density
ν	[m ² s ⁻¹]	kinematic viscosity
τ^{sgs}	[]	stress tensor

Sub- and Superscripts

i	row coordinate
j	column coordinate
n	number of samples
g	gas phase
l	liquid phase

Abbreviations

CAD	computer aided design
CFD	computational fluid dynamics
CPU	central processing unit
CUDA	computer unified device architecture
DSM	dynamic Smagorinsky model
ECT	electrical capacitance tomography
ERT	electric resistance tomography
FCT	flux corrected transport
FFT	fast Fourier transformation

FPGA	field programmable gate array
GPU	graphic processing unit
IBM	immersed boundary method
IMFT	Institute of Fluid Dynamics Toulouse
LES	large eddy simulations
MCX	micro coaxial connector
RF	radio frequency
SGS	subgrid scale
TOMOCON	smart tomographic sensors for advanced industrial process control
VoF	volume of fluid
WMS	wire mesh sensor

References

- [1] M. J. H. Simmons, J. A. Wilson, B. J. Azzopardi, *Chem. Eng. Res. Des.* **2002**, *80* (5), 471–481. DOI: <https://doi.org/10.1205/026387602320224058>
- [2] R. Fantoft, R. Akdim, R. Mikkelsen, T. Abdalla, R. Westra, E. de Haas, *SPE Annu. Tech. Conf. and Exhib.*, Society of Petroleum Engineers, **2010**. DOI: <https://doi.org/10.2118/135492 MS>
- [3] H. Liu, J. Xu, J. Zhang, H. Sun, J. Zhang, Y. Wu, *J. Hydrodyn.* **2012**, *24* (1), 116–123. DOI: [https://doi.org/10.1016/S1001-6058\(11\)60225-4](https://doi.org/10.1016/S1001-6058(11)60225-4)
- [4] L. J. A. M. van Campen, *Bulk Dynamics of Droplets in Liquid Liquid Axial Cyclones*, Ph.D. Thesis, TU Delft **2014**.
- [5] L. Ni, Z. Yin, X. Zhang, *Filtr. Sep.* **2010**, *20* (2), 24–26.
- [6] Y. Jing, *Development of Axial Flow Vane guide Cyclone Separator*, M. Sc. Thesis, China University of Petroleum, Qingdao **2010**.
- [7] W. D. Griffiths, F. Boysan, *J. Aerosol. Sci.* **1996**, *27* (2), 281–304. DOI: [https://doi.org/10.1016/0021-8502\(95\)00549-8](https://doi.org/10.1016/0021-8502(95)00549-8)
- [8] A. C. Hoffman, L. E. Stein, *Gas Cyclones and Swirl Pipes*, 2nd ed., Springer, Heidelberg **2008**.
- [9] J. J. Slot, *Development of a Centrifugal In line Separator for Oil Water Flows*, Ph.D. Thesis, University of Twente, Enschede **2013**.
- [10] S. K. Star, *Pressure distribution in a liquid liquid cyclone separator*, M. Sc. Thesis, TU Delft **2016**.
- [11] R. Knöbel, *Experimental Study on the Separation of Oil and Water Using an Axial In line Cyclone*, M. Sc. Thesis, TU Delft **2017**.
- [12] P. Airikka, *Comput. Control Eng.* **2004**, *15* (3), 18–23. DOI: <https://doi.org/10.1049/cce:20040303>
- [13] H. M. Prasser, A. Böttger, J. Zschau, A new Electrode mesh Tomograph for Gas liquid Flows, *Flow Meas. Instrum.* **1998**, *9*, 62–66. DOI: [https://doi.org/10.1016/S0955-5986\(98\)00015-6](https://doi.org/10.1016/S0955-5986(98)00015-6)
- [14] B. Sahovic, H. Atmani, P. Wiedemann, E. Schleicher, D. Legendre, E. Climent, in *Proc. of the 9th World Congress on Industrial Process Tomography*, International Society for Industrial Process Tomography, Bath **2018**, 125–134.
- [15] T. Rymarczyk, G. Klosowski, E. Kozłowski, *Sensors* **2018**, *18* (7), 2285. DOI: <https://doi.org/10.3390/s18072285>
- [16] J. L. Oschman, *Energy Medicine*, 2nd ed., Churchill Livingstone, London **2015**.
- [17] T. K. Bera, *IOP Conf. Ser. Mater. Sci. Eng.* **2018**, *331*, 12004. DOI: <https://doi.org/10.1088/1757-899x/331/1/012004>
- [18] C. Tan, Y. Shen, K. Smith, F. Dong, J. Escudero, *IEEE T. Instrum. Meas.* **2019**, *68* (5), 1590–1601. DOI: <https://doi.org/10.1109/TIM.2018.2884548>
- [19] L. Zhang, Q. Zhang, F. Zhu, in *Proc. of the 2nd Int. Conf. on Advances in Mechanical Engineering and Industrial Informatics* (Eds: M. Xu, K. Zhang), Atlantis Press SARL, Paris **2016**, 513–516.

- [20] S. Ren, J. Zhao, F. Dong, *Flow. Meas. Instrum.* **2015**, *46* (8), 284–291. DOI: <https://doi.org/10.1016/j.flowmeasinst.2015.07.004>
- [21] B. S. Kim, A. K. Khambampati, Y. J. Jang, K. Y. Kim, S. Kim, *Nucl. Eng. Des.* **2014**, *278*, 134–140. DOI: <https://doi.org/10.1016/j.nucengdes.2014.07.023>
- [22] J. Cong, Z. Fang, M. Lo, H. Wang, J. Xu, S. Zhang, in *Proc. of the IEEE 26th Ann. Int. Symp. on Field Programmable Custom Computing Machines*, IEEE, Piscataway, NJ **2018**, 2576–2621. DOI: <https://doi.org/10.1109/FCCM.2018.00023>
- [23] M. P. Escudier, J. Bornstein, T. Maxworthy, *Proc. R. Soc. London, Ser. A* **1982**, *382* (1783), 335–360. DOI: <https://doi.org/10.1098/rspa.1982.0105>
- [24] O. Kitoh, *J. Fluid. Mech.* **1991**, *225* (1), 445–479. DOI: <https://doi.org/10.1017/S0022112091002124>
- [25] G. J. de Zoeten, *Mechanistic Model of an In line Liquid liquid Swirl Separator*, B. Sc. Thesis, TU Delft **2018**.
- [26] T. Das, J. Jäschke, *IFAC PapersOnLine* **2018**, *51* (8), 138–143. DOI: <https://doi.org/10.1016/j.ifacol.2018.06.368>
- [27] S. V. Alekseenko, P. A. Kuibin, V. L. Okulov, S. I. Shtork, *J. Fluid. Mech.* **1999**, *382*, 195–243. DOI: <https://doi.org/10.1017/S0022112098003772>
- [28] T. Abadie, J. Aubin, D. Legendre, *J. Comput. Phys.* **2015**, *297*, 611–636. DOI: <https://doi.org/10.1016/j.jcp.2015.04.054>
- [29] C. S. Peskin, *J. Comput. Phys.* **1977**, *25*, 220–252. DOI: [https://doi.org/10.1016/0021-9991\(77\)90100-0](https://doi.org/10.1016/0021-9991(77)90100-0)
- [30] B. Bigot, T. Bonometti, O. Thual, L. Lacaze, *Comput. Fluids* **2014**, *97*, 126–142. DOI: <https://doi.org/10.1016/j.compfluid.2014.03.030>
- [31] I. Calmet, J. Magnaudet, *Phys. Fluids* **1997**, *9*, 438–455. DOI: <https://doi.org/10.1063/1.869138>
- [32] A. Chouippe, E. Climent, D. Legendre, C. Gabillet, *Phys. Fluids* **2014**, *26*, 043304. DOI: <https://doi.org/10.1063/1.4871728>

DOI: 10.1002/cite.201900172

Controlled Inline Fluid Separation Based on Smart Process Tomography Sensors

B. Sahovic, H. Atmani, M. A. Sattar, M. M. Garcia, E. Schleicher, D. Legendre, E. Climent, R. Zamanski, A. Pedrono, L. Babout, R. Banasiak, L. M. Portela, U. Hampel*

Research Article: Multiphase flow entering an inline fluid separation system can be measured fast and precise with a wire mesh sensor. A vortex shaped gas core, as a response of such system, can be quantified using an electrical resistive tomography sensor. In this study, both sensors together with a fast data processing hardware are part of a concept to control fluid separation. ■

